ELSEVIER

International Journal of Mass Spectrometry 195/196 (2000) 685–697

International Journal of Mass Spectrometry

Conformations of biopolymers in the gas phase: a new mass spectrometric method

Andrew C. Gill[a,1], Keith R. Jennings[a], Thomas Wyttenbach[b], Michael T. Bowers[b,*]

[a]*Department of Biological Sciences, University of Warwick, Coventry CV4 7AL, UK*
[b]*Department of Chemistry, University of California, Santa Barbara, CA 93106, USA*

Received 22 October 1999; accepted 28 October 1999

Abstract

A method is developed for measuring collision cross sections of gas-phase biomolecules using a slightly modified commercial triple quadrupele instrument. The modifications allow accurate stopping potentials to be measured for ions exiting the collision region of the instrument. A simple model allows these curves to be converted to cross sections. In order to account for certain poorly defined experimental parameters (exact ion energy, absolute pressure in the collision cell, etc.) variable parameters are included in the model. These parameters are determined on a case by case basis by normalizing the results to the well known cross section of singly charged bradykinin. Two relatively large systems were studied (cytochrome *c* and myoglobin) so comparisons could be made to literature values. A number of new peptide systems were then studied in the 9–14 residue range. These included singly and doubly charged ions of luteinizing hormone releasing hormone (LHRH) substance P, and bombesin in addition to bradykinin. The experimental cross sections were in very good agreement with predictions from extensive molecular dynamics modeling. One interesting result was the experimental observation that the cross section of the doubly charged ions of LHRH, substance P, and bombesin were all smaller than those of the corresponding singly charged ions. Molecular dynamics did not reproduce this result, predicting doubly charged cross sections of the same magnitude or slightly larger than for the singly charged species. The experimental results appear to be correct, however. Possible shortcomings in the modeling procedure for multiply charged ions were suggested that might account for the discrepancy. (Int J Mass Spectrom 195/196 (2000) 685–697) © 2000 Elsevier Science B.V.

Keywords: Biopolymers; Gas phase; Mass spectrometry; Collision cross sections

1. Introduction

One of the most important properties of a biopolymer is its three-dimensional conformation. For polypeptides and proteins, the overwhelming emphasis has been on determining condensed phase structures, primarily by x-ray diffraction [1] and multidimensional nuclear magnetic resonance (NMR) [2]. The historical reasons for this preference are twofold: first the condensed phase allows much greater molecular density and hence larger signals and second, it is presumed that such condensed-phase structures bear resemblance to the biologically active form of the molecule. While the first reason is unquestionably

* Corresponding author. E-mail: bowers@chem.ucsb.edu

[1] Present address: Institute for Animal Health, Newbury, RG20 7NN, UK.

Dedicated to Bob Squires for his many seminal contributions to mass spectrometry and ion chemistry.

PII S1387-3806(99)00256-0

true, the second isn't necessarily so. For example, x-ray methods require crystalline environments, a situation clearly not like that found in nature. In like manner, the solvent situation for most NMR experiments usually bears only a remote resemblance to true biological conditions. How protein structures change, as environmental conditions are changed, may depend strongly on the individual protein and is not yet understood.

More recently, H/D exchange studies have emerged as an important compliment to x-ray and multidimensional NMR. Initially, NMR methods [3] were developed that allowed determination of "exposed" amide hydrogens by observing their H/D exchange in solution. Subsequently, mass spectrometry has begun to play a major role in conformational analysis using H/D exchange with protocols developed for both solution [4,5] and gas phase [6] studies. While still in their infancy, mass spectrometry methods appear to be extremely powerful due to their very high sensitivity and near universal utility.

The fact that information is now becoming available on preferred gas-phase conformations of biopolymers is interesting and important. In a fundamental sense, one would ideally like to know the intrinsic solvent-free conformational preferences of peptides and proteins as benchmarks for understanding how they respond to more complex environments. If the solvent environment could be added gradually, and conformational information obtained, then great strides would be made toward eventual molecular level understanding of the biologically active medium. The first step in this process is to further develop methods for obtaining structural information in the solvent-free gas phase.

The H/D exchange experiments mentioned earlier are a step in this direction. Other, more direct and potentially more powerful methods also are being developed. It is well known that the collision cross section of a molecule is directly correlated with its structure. This truism has led to the development of several collisional methods for extracting structural information. The first of these involves determination of collisional cross sections for mass-selected ions under relatively low pressure collision conditions [7,8]. Typically, ions are formed by electrospray, mass selected, impacted on neutral gas in a collision cell, and then detected with a second mass spectrometer. A version of this experiment will be the focal point of this article and more details will be given.

The second method is based on ion mobility and hence is a high pressure method. In this case ions are formed, usually mass selected, pulse injected into a collision cell, and an arrival time distribution obtained following a second mass spectrometer. Originally the method was applied to carbon cluster conformations [9], but more recently conformations of both small [10,11] and larger sized [12,13] synthetic and biopolymers have been analyzed. An important aspect of this method is extensive molecular dynamics modeling that allows insight into the details of the low-energy conformations.

It appears the ion mobility-based methods provide great promise. However, they have the drawback of requiring one-of-a-kind research instruments that are expensive to build and difficult to operate. In this article we intend to show that rather simple modifications to a common commercial mass spectrometer can provide structural information. While it is too soon to tell if the method will be applicable generally, the results on the several systems reported here are promising.

2. Methods

2.1. Mass spectrometry

All mass spectrometry was performed on a Quattro II tandem quadruple instrument (Micromass, Altrincham, UK) equipped with an atmospheric pressure nebuliser-assisted electrospray source. All chemicals were obtained from Sigma/Aldrich and were used without further purification. Peptide solutions were made to approximately 5 pmoles/μL in water:acetonitrile 1:1 with 0.1% formic acid. The sample solutions were delivered to the electrospray source by means of a syringe pump (Harvard Instruments) at a flow rate of 5 μL/min. For all experiments argon was

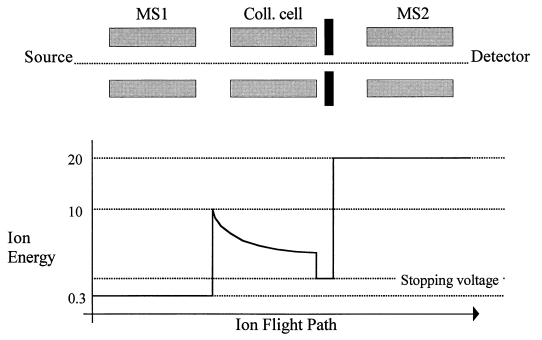

Fig. 1. Schematic of the mass analyzer region of the Quatro II mass spectrometer. The lower portion of the figure gives the ion energy for a specific value of the stopping voltage applied to the lens following the collision cell.

used as the collision gas. A schematic diagram of the instrument is given in Fig. 1.

2.2. Experimental measurement of collision cross sections

Gas phase ions were generated by electrospray ionization and passed through MS1, operated in the rf-only mode, at a nominal translation energy of 0.3 eV. They were subsequently introduced into an rf-only hexapole collision cell containing a variable pressure of argon collision gas at a translational energy of $10i$ eV, where i is the number of discrete electronic charges on the ion. The Quattro II instrument includes a lens at the exit from the collision cell, whose voltage can be varied independently of that applied to the collision cell. The voltage applied to this lens is termed the stopping voltage and was varied between 0 and 10 V in 64 steps. Ions having greater translational energy than the stopping voltage will pass this lens. Those ions that pass are accelerated to 20 eV and enter MS2 where mass separation takes place. The translational energy profile of ions passing through the mass spectrometer is shown in the lower half of Fig. 1. MS2 was scanned repetitively over a window of 10 Thomsons, centered on the mass-to-charge ratio of the ion of interest, with the results of each scan saved to disk. For each stopping voltage, the scans were summed and the normalized intensity plotted against the stopping voltage. This procedure was repeated for a range of collision cell pressures. An example is given in Fig. 2 for the 2+ ion of bradykinin.

2.3. Theoretical model of the measurement of collision cross sections

The translational energy E_1 of an ion, after a scattering collision with a neutral, is given by [14]

$$E_1 = \frac{E_0}{(m_i + m_n)^2}(m_i^2 + m_n^2 + 2m_i m_n \cos\theta_{\mathrm{CM}}) \qquad (1)$$

where E_0 is the translational energy prior the collision, m_i and m_n are the masses of the ion and the neutral, respectively, and θ_{CM} is the scattering angle in center-of-mass coordinates. For many ions having each undergone a collision, the average value of θ will be 90° and Eq. (1) will be reduced to

$$E_1 = E_0\left(\frac{m_i^2 + m_n^2}{(m_i + m_n)^2}\right) \qquad (2)$$

Since the term in brackets in Eq. (2) is a constant, the translational energy E_t of an ion that has experienced t collisions is given by this term raised to the power t

$$E_t = E_0\left(\frac{m_i^2 + m_n^2}{(m_i + m_n)^2}\right)^t \qquad (3)$$

The average number of collisions an ion will experience as it passes through the collision cell is given by

$$\bar{t} = zd\sigma \qquad (4)$$

where z is the number density of gas molecules, d is the flight path of the ions in centimeters, and σ is the collision cross section of the ion. The exact flight path of the ions is unknown but is approximated by the length of the collision cell, in this case 16 cm. For an rf-only hexapole collision cell, calculations suggest that ions are confined to a volume close to the axis [15] so this approximation is reasonable. To convert Eq. (4) into an expression containing the measured gas cell pressure, the number density of gas molecules z may be defined further as

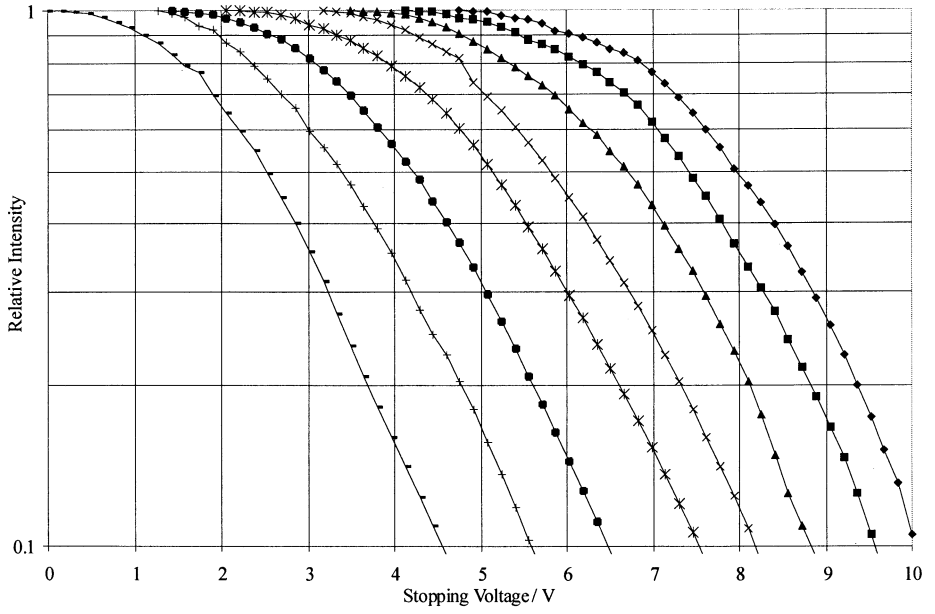

Fig. 2. A series of plots of the relative intensity of the doubly charged ion of bradykinin vs the stopping voltage for pressure gauge readings of 6×10^{-4}, 7×10^{-4}, 8×10^{-4}, 9.6×10^{-4}, 1.1×10^{-3}, 1.3×10^{-3}, 1.6×10^{-3}, and 1.9×10^{-3} mbar. The lowest pressure line is on the right of the plot.

$$z = \frac{N_A p}{24790} \tag{5}$$

where N_A is Avodadro's number, p is the gas pressure in bars, and 24 790 is the number of cubic centimeters occupied by one mole of a gas at standard temperature and pressure.

The average translational energy of an ion as it leaves the collision cell $\bar{E}_x$ is therefore given by

$$\bar{E}_x = E_0 \left(\frac{m_i^2 + m_n^2}{(m_i + m_n)^2} \right)^{N_A p d \sigma / 24790} \tag{6}$$

or

$$\log\left(\frac{\bar{E}_x}{E_0} \right) = \frac{N_A p d \sigma}{24790} \log\left(\frac{m_i^2 + m_n^2}{(m_i + m_n)^2} \right) \tag{7}$$

2.4. Fitting the theory to the measured average translational energies

Three corrections must be made to Eq. (7) to account for: (1) the fact the initial translational energy is slightly more than $10i$ eV, since ions leaving the electrospray source have a small positive translational energy; (2) the collisional gas pressure indicated on the penning gauge is not a true representation of the actual pressure inside the cell; and (3) the ion path length through the collision cell is not precisely 16 cm, the collision cell length. The modified equation becomes:

$$\log\left(\frac{\bar{E}_x}{E_0} \right) = a + b \frac{N_A p d \sigma}{24790} \log\left(\frac{m_i^2 + m_n^2}{(m_i + m_n)^2} \right) \tag{8}$$

The values of the two correction factors, a and b, were obtained by the use of a calibrant ion. Wyttenbach et al. [10a] used the ion mobility-based ion chromatography approach to investigate the gas-phase conformation of the singly protonated ion of bradykinin and measured a collision cross section for this ion of 245 Å^2. For each ion under investigation for which stopping curves were recorded, stopping curves also were recorded for the 1+ ion of bradykinin. The average translational energies from these curves were used to set the values of the correction factors by fitting Eq. (8) to the bradykinin data points. After

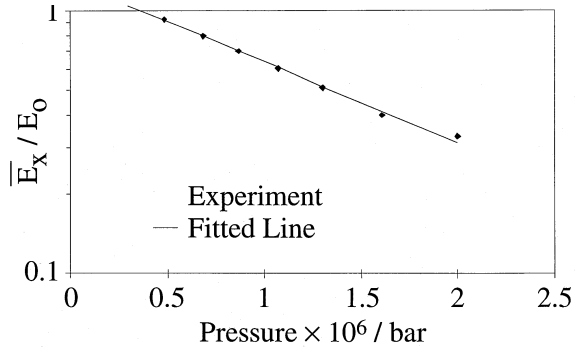

Fig. 3. A plot of $\bar{E}_x/E_0$ vs collision cell pressure gauge readings for the doubly charged ion of bradykinin. $\bar{E}_x$ is the average energy of an ion leaving the collision cell after entering with energy E_0.

fixing the values of *a* and *b*, a line was fitted to the data for each new ion under investigation by varying the collision cross section. Therefore, the measured collision cross sections in the work are effectively measured relative to that of the singly charged ion of bradykinin. Such a fit is shown in Fig. 3 for the doubly charged ion of bradykinin.

2.5. Molecular modeling

Molecular modeling calculations made use of the Amber suite of programs [16]. A simulated annealing approach, based on molecular dynamics and similar to that used by Wyttenbach et al. [10a], was used to generate low-energy conformations. An energy-minimized starting structure was heated to 800 K and allowed to equilibrate for 30 ps. The structure was then cooled to 0 K over 10 ps, the resulting structure energy minimized at 0 K, and the coordinates and energy saved to disk. The process was then repeated until 100 such structures had been generated. The collision cross sections of the energy-minimized structures were calculated using Monte Carlo methods [9,10b]. A plot of cross section versus energy for these 100 structures is termed a scatter plot [10a].

3. Results

3.1. Myoglobin and cytochrome c

These two systems were chosen to allow comparison with data in the literature. The results are given in Table 1. For cytochrome *c* there is relatively good agreement between our results and the ion-mobility results of Shelimov et al. [12] but less good agreement with the Covey and Douglas results [7a]. This is perhaps an unexpected circumstance since our methods are quite similar to those of Covey and Douglas.

Table 1
Experimental collision cross sections for myoglobin and cytochrome *c* (Å^2)

Peptide	Charge state	*m/z*	This work	Literature
Myoglobin	+9	1884	3340	2570[a]
	+10	1696	3575	—
	+11	1542	3755	3020[a]
	+13	1305	4010	3550[a]
	+14	1212	4180	—
	+15	1131	4270	4040[a]
	+17	998	4330	4290[a]
	+18	943	4435	—
Cytochrome *c*	+8	1546	2470	2100[b]
	+9	1374	2680	2370[a]/2250[b]
	+12	1031	2760	3230[a]/2400[b]
	+14	884	2765	3830[a]/2500[b]
	+15	825	2790	2600[b]
	+16	773	2965	3450[a]/2700[b]

[a] Cross section taken from [7a].
[b] Approximate cross sections taken from [12].

Table 2
Experimental and theoretical cross sections (Å^2) for a series of peptides

Peptide	Charge state	*m/z*	Cross sections	
			Experiment	Theory[a]
Bradykinin	1+	1061	245[b] (239)[c]	236 ± 5
	2+	531	255 (240)[c]	241 ± 5
Substance P	1+	1348	305	298 ± 10
	2+	679.5	285	299 ± 10
LHRH	1+	1182	275 (262)[d]	260 ± 15
	2+	591.5	240	259 ± 10; 302 ± 7
Bombesin	1+	1620	365	326 ± 15
	2+	810.5	295	339 ± 20; 384 ± 10

[a] Average of 10 lowest-energy structures.
[b] All cross sections are relative to this value from [10a] (see text).
[c] From [19].
[d] From [20].

As outlined earlier, however, we establish two fitting parameters to our stopping curves by comparison with bradykinin results. This allows correction for poorly known instrument parameters. Perhaps this is the origin of the difference, since Covey and Douglas do not reference their results to a relatively well established value. The good agreement with the ion mobility studies for cytochrome *c* suggests our approach has merit.

What is surprising is the Covey–Douglas cross sections for cytochrome *c* are substantially larger than ours or those of Shelimov et al. and that they increase much more rapidly with charge state. At the highest reported charge state (20+), Covey and Douglas report a cross section of 4310 Å^2 and Shelimov et al. 2950 Å^2. An upper limit to the cross section of ~3400 Å^2 is estimated by Shelimov et al. by calculating the cross section of an extended string model of cytochrome *c*. Hence, it appears there is a problem with either the measurement or data analysis used by Covey and Douglas. This is of some concern to us, due to the similarity of their method to ours.

What can be deduced from these results is that the cross sections monotonically increase with charge state for these two proteins, as observed by others, presumably due to increased Coulomb repulsion resulting in unfolding of the backbone. This unfolding is substantial for the charge states reported here since the calculated cross section of the x-ray structure [17] and the solution NMR structure [18] is about 1350 Å^2 [12]. However, the results of Shelimov et al. indicate the lowest charge states they investigated (3+ to 5+) are substantially more compact than the native structure with cross sections of ~1200 Å^2. Hence, charge can serve to both contract structure and eventually expand structure as it increases. More will be said about this characteristic later.

3.2. Bradykinin

Bradykinin (BK) is a nonapeptide with sequence Arg-Pro-Pro-Gly-Phe-Ser-Pro-Phe-Arg. Its gas-phase conformation has been thoroughly studied using a combination of ion mobility measurements and molecular dynamics calculations [10a]. As noted, the cross section of the singly charged ion has been used as a reference for all data reported here.

The stopping curves for the doubly charged BK are given in Fig. 2. Fitting these curves yields a cross section of 255 Å^2. Since this value is obtained relative to the assumed value of 245 Å^2 for singly protonated BK, adding a proton causes the peptide to elongate slightly, but it apparently maintains the same general shape. These results are listed in Table 2. Also given are flow tube ion mobility results of Counterman et al.

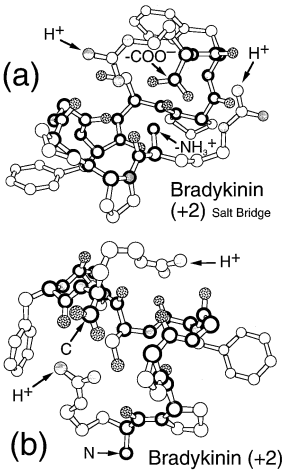

Fig. 4. Ball-stick plots of typical low-energy structures for the doubly charged ion of bradykinin: (a) salt-bridge form and (b) charge-solvation form. The atoms on the backbone are outlined in black. Carbon atoms are shown as clear circles, nitrogen as gray, and oxygen as speckled. For clarity, the hydrogen atoms are not shown. Sites of side chain protonation are indicated by H^+ and N = terminus protonation by $–NH_3^+$. The deprotonated C-terminus is labeled as $–COO^-$. For nonsalt bridge structure, N and C denote the N-terminus and C-terminus, respectively.

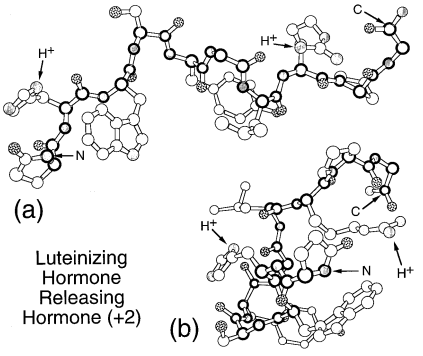

Fig. 5. Ball-stick plots of typical low-energy structures of doubly charged LHRH: (a) an open structure and (b) a compact structure. See Fig. 4 legend for atom identification.

[19], which are in acceptable agreement with both the data reported here for doubly charged BK and the singly charged result of Wyttenbach et al. [10a].

Scatter plots, relative energy versus cross section, of 100 stable structures were generated for doubly charged BK using the Amber molecular dynamics programs and the protocol of Wyttenbach et al. [10a]. Plots were obtained for two different charge distributions: both distributions had Arg1 and Arg9 protonated but one also was a salt bridge structure where the C-terminus was deprotonated and the N-terminus was protonated. While the scatter plots were somewhat different, the average low-energy cross sections were very similar. Hence, only one value is given in Table 2, and experiment cannot distinguish between them. Representative low-energy structures for the two species are given in Fig. 4. For the salt bridge form the deprotonated C-terminus is centrally located and surrounded by the three positively charged sites. For the charge solvated structure [Fig. 4(b)], the two protonated guanadine groups are located on the surface on opposite sides of the structure with the maximum possible number of carbonyl oxygens between them. The flexibility of the Arg side chains is critical in the formation of these compact structures.

3.3. Luteinizing hormone releasing hormone

Luteinizing hormone releasing hormone (LHRH) is a decapeptide with the sequence pGlu-His-Trp-Ser-Tyr-Gly-Leu-Arg-Pro-Gly-NH_2 where pGlu is pyroglutamic acid and the C-terminus is amidated. Consequently, LHRH cannot form salt bridges. Stopping voltage curves were obtained for both the 1+ and 2+ charge states with the fits yielding the cross sections given in Table 2. Of note is the fact that the 2+ charge state appears to have a smaller cross section than the singly charge ion; an unusual effect given the rather small size of LHRH and the general wisdom that Coulomb repulsion between charge centers should elongate the structure. The 1+ result is in reasonable agreement with an unpublished ion mobility study from our lab [20].

Scatter plots of 100 structures were obtained for both charge states. Similar to BK, the Arg residue is protonated in both instances and the His residue is protonated in the 2+ species. The average cross sections of the 10 lowest-energy structures of each are given in Table 2. Of interest is the fact that two distinct structural types with radically different cross sections were observed for the 2+ charge state. Examples of these two structures are given in Fig. 5. Also of interest is

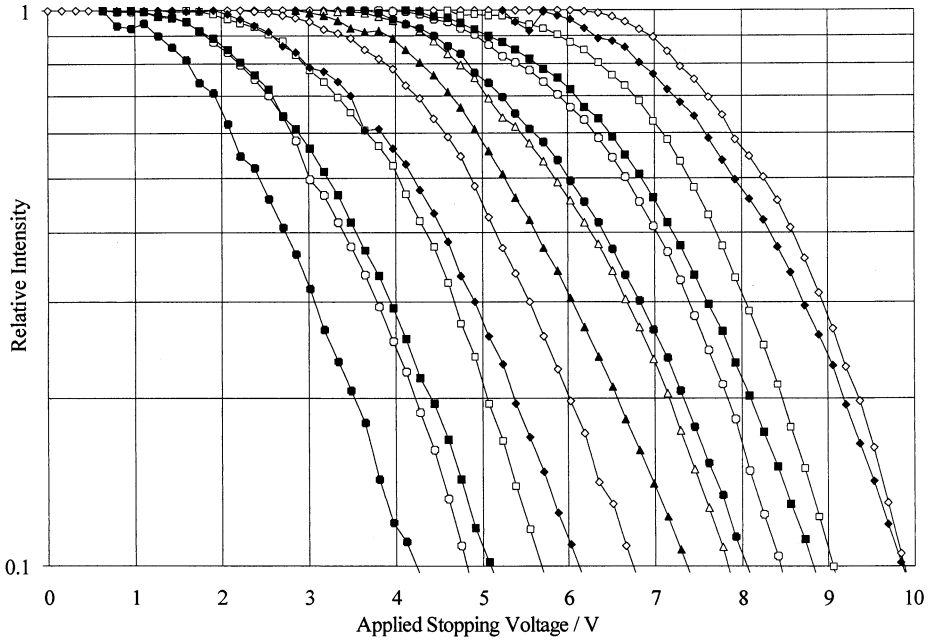

Fig. 6. Plots of relative intensity vs stopping voltage for singly charged (filled symbols) and doubly charged (open symbols) substance P for collision cell pressure gauge readings of 6.5×10^{-4}, 8×10^{-4}, 9.1×10^{-4}, 1×10^{-3}, 1.2×10^{-3}, and 1.7×10^{-3} mbar. The lowest pressure lines are on the far right of the graph.

the fact that the more compact structure appears to have about the same cross section as the 1+ species in mild disagreement with experiment.

The two structures in Fig. 5, although seemingly very different, are actually quite similar. In the compact structure Gly^6 orients such that backbone folding occurs while, for the elongated structure, Gly^6 rotates to open up the peptide. While some charge site-carbonyl oxygen interactions change upon isomerization, these are minimal.

3.4. Substance P

Substance P is an eleven-residue peptide with the sequence: Arg-Pro-Lys-Pro-Gln-Glu-Phe-Gly-Leu-Met-NH_2, where the C-terminus is amidated. Hence, substance P cannot form salt bridge structures. The stopping curves for the 1+ and 2+ charge states are given in Fig. 6. The data show quite clearly that the doubly charged species requires more voltage to "stop it" at every pressure, indicating it has a smaller cross section than the singly charge species. The cross sections from the fits are given in Table 2.

Scatter plots were calculated for both species. In both cases the Arg residue was protonated, while the Lys residue was also protonated in the 2+ ion. The average cross sections of the 10 lowest-energy structures are given in Table 2 with good agreement with experiment. The lower cross section observed for the 2+ state was not found in the calculations where essentially the same cross section was observed for both charge states. Representative low-energy structures are given in Fig. 7. The 2+ structure [Fig. 7(b)] is similar to the charge solvation structure for BK [Fig. 4(b)] with the charge sites on the surface. The singly charged structure, however, has the charge site buried in the center of the peptide where maximum solvation can occur.

3.5. Bombesin

Bombesin is the largest system studied where both experimental and detailed theoretical cross sections

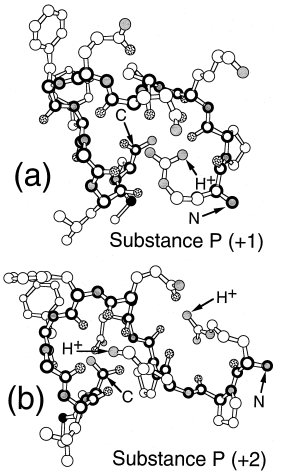

Fig. 7. Ball-stick plots of typical low-energy structures for: (a) singly charged and (b) doubly charged substance P. See Fig. 4 legend for atom identification.

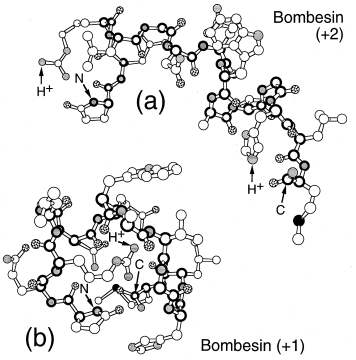

Fig. 8. Ball-stick plots of typical low-energy structures for: (a) doubly charged and (b) singly charged bombesin. See Fig. 4 legend for atom identification.

are obtained. It is a 14 residue peptide with the sequence: pGlu-Glu-Arg-Leu-Gly-Asn-Glu-Trp-Ala-Val-Gly-His-Leu-Met-NH_2. Again, no salt bridge structures are possible for this peptide. Stopping curves were obtained for the 1+ and 2+ charge states with the results given in Table 2. Like LHRH and substance P, bombesin appears to contract with the addition of a second proton.

Scatter plots were obtained for both charge states with the average cross sections of the 10 lowest-energy structures given in Table 2. The Arg residue was protonated in both cases and the His residue also protonated in the 2+ ion. Like LHRH, two low-energy forms of doubly charged bombesin were obtained in the calculations as indicated in Table 2. Representative low-energy structures are given in Fig. 8 for the two charge states. Agreement between the calculation and experiment is not as good for bombesin as for the other three peptides studied here. The general structural characteristics of the low energy species are similar to BK, LHRH, and substance P.

4. Discussion

One of the most surprising aspects of this work is the observation that the doubly charged ions of LHRH, substance P, and bombesin all appear to be more compact than their corresponding singly charged ions. Even in BK, the singly and doubly charged ions have about the same cross section. In these systems there are 4.5, 5, 5.5, and 7 residues per charge. In the work of Shelimov et al. on cytochrome *c*, the cross section monotonically increases with charge from the 3+ charge state (35 residues per charge) and radically increases near the 7+ charge state (15 residues per charge). Similar effects are observed for myoglobin (see Table 1) which has 16 residues per charge for the 9+ charge state.

The origin of this effect is not yet clear. If one looks at the compact structures of the 2+ charge state for BK, LHRH, and substance P (Figs. 4, 5, and 7) a common feature is apparent. The two protonated sites arrange themselves on opposite sides of the molecule with as many “negative” carbonyl oxygens oriented in between them as backbone curvature will allow. These structures are facilitated by the fact that at least one of the charge carriers in each molecule is an Arg residue with its highly flexible side chain and terminal guanadine group. The compact low-energy form of bombesin (not shown) also has the same general structure as the other three compact doubly charged peptides. The charge sites of these low-energy conformers, even though on the “surface” of the molecule, are still able to intimately interact with approximately four carbonyl oxygens providing substantial stabilization.

The singly charged species, on the other hand, all have the charge site buried in the center of the molecule (see Figs. 7 and 8 for LHRH and bombesin) with up to six carbonyl oxygens in close contact in the low-energy conformers. Hence, this is the preferred (i.e., lowest-energy) local structure for charge solvation. In the much larger systems like cytochrome *c*, for low-charge states, each charge will likely surround itself with approximately six carbonyl oxygens since plenty are available. As the charge state increases, this degree of solvation will become less possible and more elongated structures with lower carbonyl oxygen solvation numbers will result. A second effect will be encountered as well at higher charge states. Charge will be necessarily deposited on the less basic sites (which also happen to be less flexible) and on sites that are not an optimum separation from adjacent charge centers. Both effects will lead to elongation of the backbone due to decreased shielding of the charges.

One of the results of the calculations is that both LHRH and bombesin have two low-energy conformers for the 2+ charge state: a compact structure and an elongated structure (see Fig. 5 for an example). In the compact structure, the backbone is strongly folded to allow shielding of the charges. In the elongated structure, the backbone is essentially fully extended. In both cases approximately four carbonyl oxygens solvate the charge. For both LHRH and bombesin, three of the 10 lowest-energy structures are elongated with the remaining seven compact. The average cross section of the compact structures agrees much better with experiment than the cross sections of the elongated structures, suggesting that a compact conformation is the dominant species being experimentally sampled.

The possibility of multiple low-energy structures with dramatically different cross sections suggests these systems are good candidates for more detailed study. Unfortunately, the experimental method described here is a continuous beam method and cannot sort out structural variation of this type. Ion mobility methods, on the other hand, are inherently pulsed and hence measure arrival time distributions at a detector. Extended conformers with larger cross sections, would thus arrive at the detector at later times than compact conformers with smaller cross sections. The two sets of conformers found in the calculations have very different cross sections; differences of 16% (LHRH) and 13% (bombesin). In recent work on poly(ethyleneterephthalate) oligomers, we were easily able to baseline resolve conformers that differed by 10%–13% in cross section [21]. In that instance, we were also able to extract information on the barrier associated with isomerization between the two conformers by doing temperature dependent studies. Similar studies are being initiated on the peptides LHRH and bombesin and will be reported elsewhere.

One useful way to envision the folding in these systems is to catalogue the frequency with which a particular carbonyl oxygen intimately interacts with the charge site. For this purpose, all 100 structures were surveyed with an intimate interaction defined as a separation of 4.0 Å or less. The details are given in Table 3 for BK, substance P, and LHRH. Several features stand out. First, for the singly charged species, essentially all carbonyl oxygens are sampled. An unusual exception is the carbonyl oxygen of Lys^3 in substance P, which is coordinated only once in 100 structures. This surely is a result of being sandwiched between Pro^2 and Pro^4, which have very restricted folding angles due to their cyclic nature and apparently rotate the Lys^3 carbonyl oxygen away from the charge site.

The doubly charged ions show a much different picture. In all cases each charge site interacts strongly with approximately half of the carbonyl oxygens and essentially ignores the other half. Hence, the variety of structures for the doubly charged species is much smaller than for the complementary singly charged species. The number of carbonyl oxygens coordinating with the charge site in the singly charged species, averaged over all 100 structures is 3.9, 4.8, and 3.1 for LHRH, substance P, and bombesin, respectively. For the lowest-energy structures, this number approaches 6. Hence, the higher-energy conformations coordinate with fewer carbonyl oxygens. For the doubly charged species, the average number of carbonyl oxygens coordinating with a single charge site is 3.3, 2.6, 3.2, and 2.5 for BK, LHRH, substance P, and bombesin, respectively. In this case, the number approaches 4 for the lowest-energy structures. Said another way, each charge site is solvated by about 1.2 more carbonyl

Table 3
Number of times a particular carbonyl oxygen is coordinated with a specific charge site for doubly charged bradykinin, and for singly and doubly charged LHRH, and substance P for the 100 structures calculated using the annealing protocol described in the text. Coordination is defined as separation of 4.0 Å or less

Charge site		Residue of carbonyl oxygen									
	Bradykinin	Arg^1	Pro^2	Pro^3	Gly^4	Phe^5	Ser^6	Pro^7	Phe^8	Arg^9	
+2	Arg^1 (+)	65	59	42	19	14	8	2	3	3	
+2	Arg^9 (+)	2	3	32	45	34	46	72	50	26	
	LHRH	$pGlu^1$	His^2	Trp^3	Ser^4	Tyr^5	Gly^6	Leu^7	Arg^8	Pro^9	Gly^{10}
+1	Arg^8 (+)	15	30	32	40	61	62	45	27	40	41
+2	Arg^8 (+)	0	0	5	10	16	36	21	56	86	79
+2	His^2 (+)	14	86	26	38	35	7	7	4	2	2
	Substance P	Arg^1	Pro^2	Lys^3	Pro^4	Glu^5	Gln^6	Phe^7	Phe^8	Gly^9	Leu^{10}	Met^{11}
+1	Arg^1 (+)	33	83	1	57	58	40	43	28	51	64	66
+2	Arg^1 (+)	45	36	51	48	4	2	3	4	4	7	7
+2	Lys^3 (+)	2	1	7	27	57	75	59	67	63	72	70

oxygens for singly charged than for doubly charged ions. This stabilizing effect, and the minimization of Coulomb repulsion, are what drive charges to be as distant from each other as possible in larger peptides/proteins such as cytochrome *c*. In a qualitative sense, this effect explains why the five lowest charge states in cytochrome *c* are more compact than the native structure, while the higher charge states become substantially more elongated than the native structure.

The question of why experiment indicates a smaller cross section for the doubly charged species and molecular dynamics does not is puzzling. The stopping-voltage plots for LHRH, substance P, and bombesin all are qualitatively similar: The doubly charged ion requires a larger voltage "to be stopped" than the singly charged ion (see Fig. 6). Hence, the doubly charged ion must be experiencing fewer collisions and thus have a smaller cross section than the corresponding singly charged ion. This cannot be due to the interaction potential, which was ignored in the data analysis. To first order, the leading attractive term is the charge-induced dipole which indicates the cross section should increase with charge as $(i)^{1/2}$ [7a]. It is, frankly, difficult to conceive of an experimental explanation for the observed results other than that already offered; the doubly charged ions have smaller cross sections.

In the molecular dynamics simulations, the dielectric constant K is assumed to take on a single value. In vacuum the value is 1, but in liquid water it increases to 80 with values for less dense and less polar media in between. The Coulomb energy between two charged species is

$$E_C = \frac{1}{4\pi\epsilon_0 K}\frac{q_1 q_2}{r_{12}}, \tag{9}$$

where q_1 and q_2 are the charges in question, ϵ_0 is the permitivity of vacuum, and r_{12} is the distance between the charges. Therefore, at a fixed value of r_{12}

$$\frac{E_C(\text{peptide})}{E_C(\text{vacuum})} = \frac{1}{K(\text{peptide})} \tag{10}$$

since K(vacuum) is unity. Rearranging,

$$E_C(\text{peptide}) = \frac{E_C(\text{vacuum})}{K(\text{peptide})} \tag{11}$$

Since the intermediate peptide structure separating the charges isn't really a continuous dense medium, K(peptide) is a complex function of r_{12}, varying from $K(\text{peptide}) = 1$ for no peptide shielding of the charge

(i.e. at short range) to a value that could reach 10 or higher. Since E_C falls off slowly (as $1/r_{12}$), this effect should be included when modeling multiply charged peptides. It was not included here. If E_C is reduced, then most probably the overall size of the double-charged peptides predicted by the calculations will also be reduced. Since this is only one of many factors governing the final conformational state, it is not possible to determine whether it would remove the discrepancy between experiment and theory. It does work in the right direction, however.

A second effect could also be at work. In calculating cross sections, we have used energy minimized 0 K structures. In reality, the experimental peptides have some internal energy. At a minimum, a 300 K distribution should be used but the actual peptides may be somewhat hotter due to instrumental details in the electrospray ionization (ESI) source and ion handling systems. In previous studies, we have noted that heating a structure leads to a dynamically averaged cross section larger than expected from the 0 K structure [22]. This effect can be as large as 5% or greater. In heating a peptide, those carbonyl oxygens coordinated to a charge remain relatively in place while the remainder of the peptide oscillates significantly. The doubly charged system will resist expansion more since more oxygens are coordinated to charge centers and since the charge centers need to avoid each other. Hence, dynamics calculations would most likely show singly charged species becoming larger relative to the corresponding doubly charged ions. Again, a move in the right direction. Unfortunately, dynamics calculations have not yet been done on these systems because of the large amount of computer time required.

5. Summary and conclusion

A commercial triple quadruple instrument has been modified to allow accurate measurement of stopping potentials for ions exiting the collision cell. A simple model has been deduced to explain the results. Two variable parameters are included in the model to account for poorly known collision-cell pressures and ion-path lengths and for stray voltages or other systematic instrumental uncertainties. Bradykinin is used as a reference system with known cross section [10a] to allow determination of the two variable parameters for each system of interest. The system collision cross section is then determined by a series of fits to ion stopping curves.

Comparisons are made to literature data on cytochrome *c* and myoglobin. Good agreement is obtained with the ion mobility results on cytochrome *c* [12], but less good agreement with ion beam results on both cytochrome *c* and myoglobin [7a]. Some of the ion beam results are shown to be outside the range of physical possibility, although it isn't clear why they are. The agreement with the ion mobility results is encouraging.

Four peptides were studied: BK, LHRH, substance P, and bombesin. Of these, the latter three showed a common trait; the doubly charged species was more compact than the singly charged species. This is a robust experimental result. Extensive molecular dynamics modeling yielded average low-energy cross sections in good quantitative agreement with experiment. However, the doubly charged species was always calculated to be either equivalent in size or slightly larger than the corresponding singly charged ion in disagreement with experiment. Two effects not accounted for in the calculations could be responsible: the fact that the dielectric constant is probably spatially variable in doubly charged ions and that thermally averaged dynamics calculations should increase the size of singly charged ions more than doubly charged ions.

One shortcoming of the method described here is its inability to measure size distributions, especially when two distributions varying substantially in cross section may be involved. For such cases, ion mobility experiments [12,19] are required. However, the ease of measurement and the ready availability of suitable instrumentation in many laboratories make the method described here appealing, especially since we've shown that it gives reliable estimates of the cross sections of both small and large peptides.

Acknowledgements

This work was supported by the EPSRC (UK) and by NSF and AFOSR (USA). We also wish to thank Phillip Roskelly for help with the instrumentation and Clive Wilson for help with the molecular modeling calculations. Finally, this work is for you, Bob. Thanks for continuing to provide inspiration and meaning to what we do.

References

[1] T.L. Blundell, L.N. Johnson, Protein Crystallography, Academic, New York, 1976.
[2] W. Braun, Q. Rev. 19 (1987) 115; K. Wüthrich, Acc. Chem. Res. 22 (1989) 36.
[3] W.W. Englander, N.R. Kollenbach, A. Rev. Biophysics 16 (1983) 521.
[4] V. Kattu, B.T. Chait, Rapid Commun. Mass Spectrom. 5 (1991) 2141; J. Am. Chem. Soc. 115 (1993) 6317; D.L. Smith, Y. Deng, Z. Zhang, J. Mass Spectrom. 32 (1997) 135.
[5] For a recent analysis of solution H/D exchange see C. Woodward, J. Am. Soc. Mass Spectrom. 10 (1999) 627 and the five articles that follow.
[6] B.E. Winger, K.J. Light-Wahl, A.L. Rockwood, R.D. Smith, J. Am. Chem. Soc. 114 (1992) 5897; X. Cheng, C. Feuselaw, Int. J. Mass Spectrom. Ion Processes 122 (1992) 109; T.D. Wood, R.A. Chorush, F.M. Wampler III, D.P. Little, P.B. O'Connor, F.W. McLafferty, Proc. Natl. Acad. Sci. USA 92 (1995) 2451.
[7] (a) T. Covey, D.J. Douglas, J. Am. Soc. Mass Spectrom. 4 (1993) 616; (b) B.A. Collins, D.J. Douglas, J. Am. Chem. Soc. 118 (1996) 4488; (c) Y.L. Chen, B.A. Collings, D.J. Douglas, J. Am. Soc. Mass Spectrom. 8 (1997) 681.
[8] K.A. Cox, R.K. Julian, R.G. Cooks, R.E. Kaiser, J. Am. Soc. Mass Spectrom. 5 (1994) 127.
[9] G. von Helden, M.-T. Hsu, P.R. Kemper, M.T. Bowers, J. Chem. Phys. 95 (1991) 3835; G. von Helden, M.-T. Hsu, N. Gotts, M.T. Bowers, J. Phys. Chem. 97 (1993) 8182.
[10] (a) T. Wyttenbach, G. von Helden, M.T. Bowers, J. Am. Chem. Soc. 118 (1996) 8355; (b) T. Wyttenbach, J.E. Bushnell, M.T. Bowers, *ibid*. 120 (1998) 5098.
[11] G. von Helden, T. Wyttenbach, M.T. Bowers, Int. J. Mass Spectrom. Ion Processes 146 (1995) 349.
[12] K.B. Shelimov, D.E. Clemmer, R.R. Hodgins, M.F. Jarrold, J. Am. Chem. Soc. 119 (1997) 2240.
[13] D.E. Clemmer, M.F. Jarrold, J. Mass Spectrom. 32 (1997) 577; C.S. Haaglund-Hyzer, A.E. Counterman, D.E. Clemmer, Chem. Rev. (in press).
[14] D.J. Douglas, J. Phys. Chem. 86 (1982) 185.
[15] C. Hagg, I. Szabo, Int. J. Mass Spectrom. Ion Processes 73 (1986) 295.
[16] D.A. Pearlman, D.A. Case, J.C. Caldwell, G.L. Seibel, U.C. Singh, P. Weiner, P.A. Kollman, AMBER 4.0, University of California at San Francisco (1991).
[17] G.W. Bushnell, G.V. Louie, G.D. Brayer, J. Mol. Biol. 214 (1990) 585.
[18] P.X. Qi, D.L. DiStefano, and A. Ward, J. Biochem. 33 (1994) 6408.
[19] A.E. Counterman, S.J. Valentine, C.A. Srebolus, S.C. Henderson, C.S. Hoaglund, D.E. Clemmer, J. Am. Soc. Mass Spectrom. 9 (1998) 743.
[20] J. Batka, T. Wyttenbach, M.T. Bowers, unpublished data.
[21] J. Gidden, T. Wyttenbach, J. Batka, P. Weis, A.T. Jackson, J.H. Scrivens, M.T. Bowers, J. Am. Chem. Soc. 121 (1999) 1421; J. Am. Soc. Mass Spectrom. 10 (1999) 883.
[22] G. von Helden, T. Wyttenbach, M.T. Bowers, Int. J. Mass Spectrom Ion Processes 146/147 (1995) 3491.